Evaluation of the noise-exposed cochlea using synchrotron radiation-based microtomography

Soledad Levano*[a], Christine Tanner[b], Georg Schulz[b], Robin Horber[a], Timm Weitkamp[c], Bert Müller[b], Daniel Bodmer[a,d]
[a]Department of Biomedicine, University Basel Hospital, Hebelstrasse 20, 4031 Basel, Switzerland; [b]Biomaterials Science Center, Department of Biomedical Engineering, University of Basel, Hegenheimermattweg 167C, 4123 Allschwil, Switzerland; [c]Synchrotron SOLEIL, L'Orme des Merisiers, 91190 Saint-Aubin, France; [d]Clinic for Otorhinolaryngology, Head and Neck Surgery, University Basel Hospital, 4031 Basel, Switzerland

ABSTRACT

Noise-induced hearing loss can be caused by sudden or prolonged exposure to loud noise. Noise exposure is known to contribute to the degeneration of sensory cells, disrupting the conversion of mechanical sound waves into electrical impulses and further their transmission to the brain. To determine the pathophysiological condition of the inner ear cells in animal models, the measurement of the animals' hearing is essential. The follow-up examination of the cochlea is particularly important as it provides information on the cellular morphology changes. Our aim was therefore to investigate the hair cell survival in the inner ear of mice exposed to two high noise levels using synchrotron radiation-based microtomography. Its spatial resolution allows for the reconstruction of three-dimensional images of unstained cochlea at the cellular level. We segmented the basilar membrane via automatic cell segmentation and fast manual cell removal, and determined its length using a one-dimensional Isomap embedding. After extracting its middle region and image slices aligned with it, surviving inner and outer hair cell locations were semi-automatically determined and then manually corrected using the ImageJ plugin PointPicker. These results were compared with the confocal microscopy data. The data collected provides meaningful information about healthy and damaged hair cells in the adult cochlea.

Keywords: Hearing loss, noise, synchrotron radiation-based microtomography, cochlea, sensory cells

1. INTRODUCTION

The World Health Organization estimates hearing loss affects over 5 % of the world's population. Noise-induced hearing loss is a modern problem, given that we are constantly exposed to noise in and outside the workplace. The mechanosensory structures in the inner ear can recover or be permanently damaged by the noise, depending on the intensity and duration of the noise level [1]. Hair cells are specialized mechanoreceptor cells that convert mechanical sound waves into electrical impulses and transmit them to the central nervous system [2]. Cochlear hair cells consist of one row of inner hair cells and three rows of outer hair cells. Hair cells are arranged on the basilar membrane and oriented along a tonotopic axis.

After measuring the hearing of animals exposed to noise or other stress factors, a morphological examination of the cochlea is required. Microdissection of the damaged adult cochlea is a technical challenge, as the complex cochlear structure is fragile. The whole cochlear preparations are often dissected into three sections, each corresponding to one turn. After staining the sections, the cells are imaged using fluorescence microscopy [3]. The images obtained can be of high quality, but the samples are mounted flat, which means that the original three-dimensional (3D) structure and organization of the inner ear cells are lost. Imaging the entire cochlea as 3D structure at the micrometer scale was achieved using light sheet fluorescence microscopy [4]. In order to be able to analyze the cochlea, it must become transparent so that the light can penetrate the tissue better, *i.e.* the samples must undergo a tissue-clearing process. The images obtained provide the geometric organization of the intact cochlea and can be used to create a tonotopic map of the cochlea [4].

* s.levano@unibas.ch; phone +41 61 265 2525; www.bmc.unibas.ch

Developments in X-Ray Tomography XV, edited by Bert Müller, Ge Wang,
Proc. of SPIE Vol. 13152, 1315204 · © 2024 SPIE
0277-786X · doi: 10.1117/12.3028091

An alternative method for imaging the cochlea while maintaining the 3D structure is the use of synchrotron radiation-based microtomography (SR-µCT) [5-10]. This technique enables the 3D visualization of the mechanosensory structures without the need for microdissection (or staining). Using synchrotron radiation-based phase-contrast imaging, the 3D cytoarchitecture of the intact human cochlea was visualized [11]. In addition, a 3D tonotopic map of the human cochlea was created, which could be used for cochlear implant purposes [12].

In this study, we used SR-µCT to examine the auditory hair cells of healthy and noise-exposed mice. We imaged decalcified cochleae embedded in paraffin. We determined the length of the segmented basilar membrane to localize the middle cochlear region. The surviving inner and outer hair cells in the middle region were detected semi-automatically and corrected manually. This enabled us to compare the two groups. Further optimization of the semi-automatic detection process will facilitate the quantitative analysis of larger populations.

2. METHODOLOGY

2.1 Tissue preparation

All animal experiments were conducted with the approval of the Animal Care Committee of the Canton Basel City, Switzerland (No. 31195-3025). Male mice aged four to six weeks were exposed to broadband noise of 8 to 16 kHz at noise levels of 100 and 120 dB sound pressure level (SPL) for a duration of two hours to induce threshold shifts. Control mice were not exposed to the noise. After the final hearing measurements, the cochleae were isolated and fixated with paraformaldehyde. The cochleae were decalcified with MOLdecal 10 (Milestone, Biosystems, Switzerland) and embedded into paraffin using the tissue processing center TPC 15 trio (Medite, GmbH Burgdorf, Germany). One ear of each mouse was used for SR-µCT analysis and immunofluorescence staining of cochlear explants, while the other ear was used for histological examinations.

2.2 SR-µCT data acquisition

For SR-µCT imaging, paraffin-embedded specimens were punched and vertically aligned with the apex on the bottom. The SR-µCT measurements were performed at the ANATOMIX beamline at the Synchrotron SOLEIL (Saint-Aubin, France) [13]. The undulator gap of 5.7 mm and a 100 µm Cu filter were chosen to generate X rays with an effective average photon energy of about 35 keV. For tomographic imaging, 5,900 radiographic projections were recorded over an angular range of 360° with off-axis alignment to extend the horizontal field of view of the detector. The detector system consisted of a 20 µm-thick LuAG scintillator coupled to a scientific CMOS camera (Hamamatsu Orca Flash 4.0 V2, 2048 × 2048 pixels, 6.5 µm physical pixel size) via a lens system including a 10× microscope objective (Mitutoyo M PLAN APO, numerical aperture 0.28), giving an effective pixel size of 0.65 µm [14]. The sample was placed 37 mm in front of the detector to allow for edge enhancement. The exposure time was 100 ms per projection. To minimize the overhead, the fly scan mode was used. The scan time for a single height step was approximately ten minutes. Two height steps were required to capture the entire cochlea.

2.3 Microscopy acquisition

After the cochleae were imaged with the SR-µCT, the samples were deparaffinized and isolated as cochlear whole mounts as described by Montgomery *et al.* [3]. Hair cells were stained by immunofluorescence and visualized with a Nikon Eclipse Ti microscope, equipped with a Yokogawa confocal spinning unit W1, a Photometrics Prime 95B camera, and the NIS software (version 5.21, Nikon AG Instruments, Egg, Switzerland). The labeled hair cells were counted in a 400 µm section of the middle region. For histological examinations, paraffin blocks were sectioned and stained with hematoxylin-eosin using the Epredia Gemini automated slide stainer (Thermofisher Scientific, Reinach, Switzerland). Samples were imaged using Nanozoomer S60 digital slide scanner (Hamamatsu, Japan).

2.4 SR-µCT segmentation

The SR-µCT images of the two height levels were automatically stitched by determining a 3D translation, which maximized the correlation of the two images in the overlap region. Since the datasets are large with up to 3.2×10^{10} voxels in basilar membrane region and the numerous hair cells are small, a semi-automatic segmentation method for the hair cells

was developed. Only minor user interactions were required. First, bright spherical regions were automatically extracted by a combination of intensity thresholding and region feature analysis. Specifically, after intensity thresholding, (i) all connected regions were extracted via the Matlab function bwconncomp, (ii) the volume and eigenvectors of each region were determined via the Matlab function regionprops3, and (iii) only spherical regions with ratios of first to third Eigenvalue below 1.7 and volumes equivalent to spheres of diameters between 3.10 and 6.44 µm were kept. A sequence of intensity thresholds was used, namely from the mean to the 99th percentile intensity value in steps of 2,500. The accepted regions from the different thresholds were merged and their region features again checked as in step (iii). Second, the centroid positions of all accepted regions were saved and loaded into FreeCAD (version 0.19). The basilar membrane structure is evident in this point cloud and was manually segmented in less than 20 minutes per dataset. To fit into memory and focus on the basilar membrane, the images were reduced to the region and content covered by the convex hull of the segmented basilar membrane points plus a margin of ±32 µm. Third, spherical regions and their centroid positions were extracted from the segmented basilar membrane image following steps (i-iii). The 1D manifold of the basilar membrane was automatically determined via 1D Isomap embedding of the centroid positions using the Matlab dimensionality reduction toolbox from van der Maaten *et al.* [15]. The basilar membrane length was calculated based on the smoothed centerline obtained by fitting a 20D polynomial to the mean positions of 301 partitions according to the embedding distance. The middle region of the basilar membrane, which accounts for 45 to 75 % of the length measured from the apical tip, was extracted. Fourth, the inner and outer hair cells of this middle region were extracted based on (i) manually selecting centroid points along visually recognizable 1D curves, (ii) fitting a spline to these selected points and (iii) accepting all centroid points within a certain distance to this spline. The distance threshold was determined semi-automatically based on visually inspecting the histogram of distances, which showed clear clustering. Fifth, images were resliced to be aligned with the outer hair cells. Four slices were combined by maximum intensity projection to reduce correction time and the corresponding centroid pixel positions of the inner and outer hair cell were written to files for manual corrections with the ImageJ plugin PointPicker. Sixth, the image sequences were imported into the ImageJ software as *z*-stacks. The text file with the positions of the inner or outer hair cells was loaded into the PointPicker plug-in window. When scrolling through the *z*-stacks, the hair cells appeared first and then the support cells. Therefore, the first (aligned) landmarks that appeared in the *z*-stacks were accepted as inner or outer hair cells, while the landmarks that appeared later were discarded.

3. RESULTS AND DISCUSSION

We evaluated the initial scans of decalcified and non-decalcified cochleae immersed in phosphate-buffered saline (PBS) or in 70 % ethanol, or embedded in paraffin to determine the adequate embedding for image acquisition. The best quality images were obtained with decalcified cochleae embedded into paraffin. The images acquired with SR-µCT provided clear visualization of the structural details of the cochlear compartments and cells, similar to that reported in previous works examining human [5, 10-12], or laboratory animal specimens [6-9, 16]. In earlier publications, the microstructures of the cochlea were identified in osmium tetroxide-stained samples with a resolution of 3 to 4 µm [6-9]. In the paraffin-embedded samples, we achieved a spatial resolution better than 1 µm, which allowed both identifying the microstructures and quantifying the hair cell numbers. In two studies, cochleae of guinea pigs exposed to noise were examined [7, 9]. In one study, the visualization of nerve fiber bundles was improved by using osmium tetroxide as post-fixation [7]. In the second study, regions of hair cell and nerve fiber loss were detected, but quantification was performed using classical histology [9]. In general, one can agree that the method based on X-ray microtomography is less time-consuming and offers multiple options for cochlear analysis.

On average, 79,461 cells per cochlea were automatically segmented. From these, cells outside the basilar membrane structure were removed, which resulted in 10,727 remaining cells per cochlea. The length of the basilar membrane ranged from 5.60 to 6.29 mm, see Table 1. An example of the segmented basilar membrane with cells of the middle region is shown in Figure 1.

A range of 546 to 1433 outer hair cells and 242 to 1223 inner hair cells were semi-automatically segmented in the *z*-stacks for correction, see Table 2. An example of labeling the inner hair cells as landmarks in the *z*-stacks for counting is shown in Figure 2. After the manual correction using PointPicker, 268 to 734 outer hair cells and 190 to 238 inner hair cells were labeled, see Table 2.

Table 1. Sample characteristics and cell segmentation.

Samples	Noise (dB SPL)	Length basilar membrane (mm)	*z*-stack slices	Detected cells	
				Automatic detention	Fast manual correction
Sample 1	0	6.20	84	112,523	12,700
Sample 2	0	6.20	138	44,921	8,769
Sample 3	100	6.26	87	118,197	12,496
Sample 4	100	6.28	174	58,639	10,720
Sample 5	120	6.29	157	63,702	8,399
Sample 6	120	5.60	175	78,782	11,279
Mean±SD				79,461 ± 29,896	10,727 ± 1,821

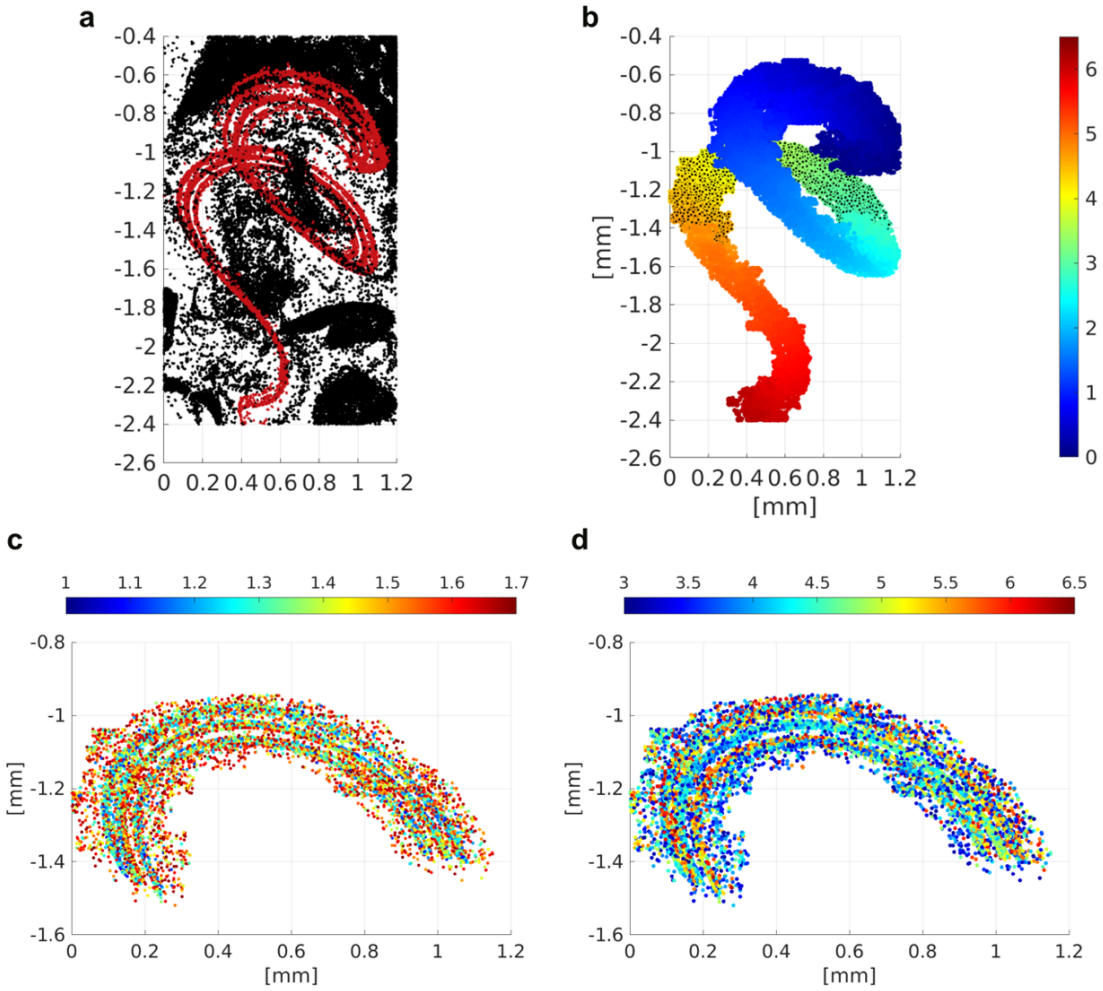

Figure 1. Basilar membrane segmentation of Sample 3. (Video 1: a) Automatically segmented cells (black and red) and cells highlighted in red along the basilar membrane region after fast cell removal. **http://dx.doi.org/10.1117/12.3028091.1** (b) Segmented basilar membrane with color-encoded visualization of embedding length from apical to basal region, with a total length of 6.26 mm. Segmented cells in the middle region are marked by black dots. (c, d) Cells of the middle region with color encoding (c) ratio of first to third Eigenvalue (accepted if < 1.7), (d) cell diameter in µm (accepted if between 3.1 and 6.4 µm).

Table 2. Inner and outer hair cell counting.

Samples	Noise (dB SPL)	Fast manual correction			PointPicker manual correction			Immunofluorescence		
		OHC	IHC	OHC /IHC	OHC	IHC	OHC /IHC	OHC	IHC	OHC /IHC
Sample 1	0	1,249	1,223	1.02	734	238	3.08	169	50	3.38
Sample 2	0	1,185	242	4.90	723	213	3.39	169	51	3.31
Sample 3	100	1,188	290	4.10	625	214	2.92	163	50	3.26
Sample 4	100	1,433	461	3.11	695	218	3.19	164	50	3.28
Sample 5	120	775	220	3.52	280	226	1.24	8	45	0.18
Sample 6	120	546	510	1.07	268	190	1.41	NA	NA	NA

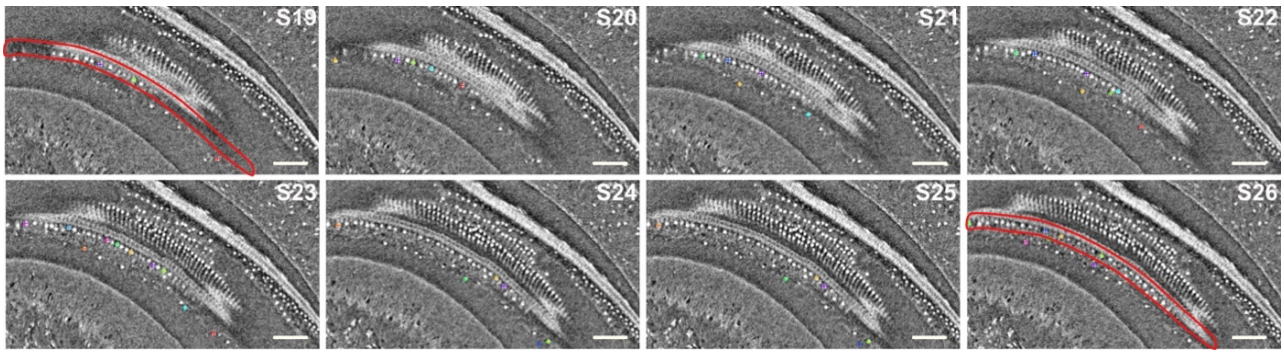

Figure 2. The *z*-stack series of a section of the middle region from Sample 1 as shown in the PointPicker plugin. All cells identified by a semi-automatic segmentation method in the area of the inner hair cells are marked with a colored "+". The red manual annotation delimited the region of the inner hair cells. S corresponds to the slide number. The scale bars are 50 µm.

The hair cell counts from untreated samples were analyzed for the SR-µCT data and the immunofluorescence data. The ratio of outer and inner hair cells (OHC/IHC) of the middle region of the basilar membrane, calculated from the SR-µCT data, was similar for both samples, see Figure 3 and Table 2. The hair cell counting of the immunofluorescence samples in a 400 µm-thick section of the middle region was also similar for both untreated samples. The OHC/IHC ratio between the two methods was similar, confirming a ratio of 1 to 3, meaning that there is approximately 3 OHC for every IHC.

The hair cell counts from the treated samples were compared for the SR-µCT data and the immunofluorescence data (Figure 4, Table 2). The samples from mice exposed to a lower noise level of 100 dB SPL showed few hair cell losses, which were correctly detected by both methods resulting in an OHC/IHC ratio of about 3. It is known that a high noise level of 120 dB SPL triggers hair cell death, so we expected a high loss of hair cells. In these samples exposed to 120 dB SPL, it was a challenging task to identify the bright spherical particles belonging to the hair cells. Also, the supporting cells were identified as bright spherical particles, thus it was difficult to distinguish between hair cells and supporting cells. However, the knowledge that the supporting cells are localized at a different plane than the hair cells helped to identify the cell types. Compared to about 2 hours for the correction of untreated samples, an extensive manual correction of about 10 hours was required to determine the number of surviving hair cells on SR-µCT. Using immunofluorescence, very few hair cells were detected in one sample, while no cells were found in the other sample (NA). The high rate of hair cell loss probably made the sensory epithelium sensitive to external intervention, so most of the remaining surviving hair cells were lost during the procedures. This suggests that the data from SR-µCT provide a better estimate of the remaining hair cells. Similar morphological features of the cochlear samples were determined by SR-µCT and histology (Figure 5).

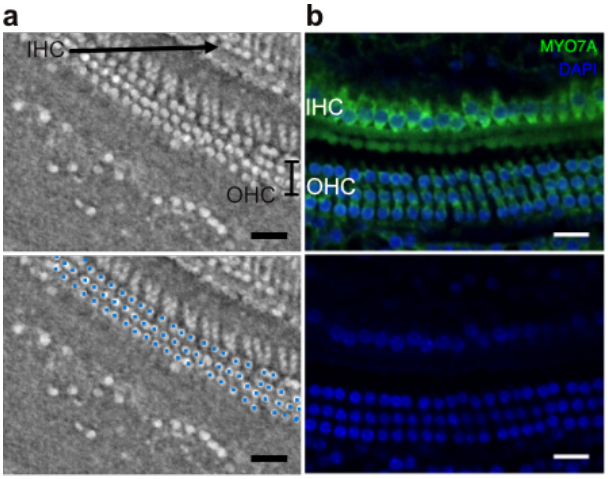

Figure 3. Images of the middle region of Sample 1 showing outer hair cells using SR-µCT (a) and immunofluorescence microscopy (b). (a) An example of the average of three *z*-stacks with a corrected version of the labeled outer hair cells is shown below. (b) A single *z*-stack image of the stained hair cells (green) and their nuclei (blue). MYO7A=Myosin 7a. IHC = inner hair cells. OHC = outer hair cells. The scale bars are 20 µm.

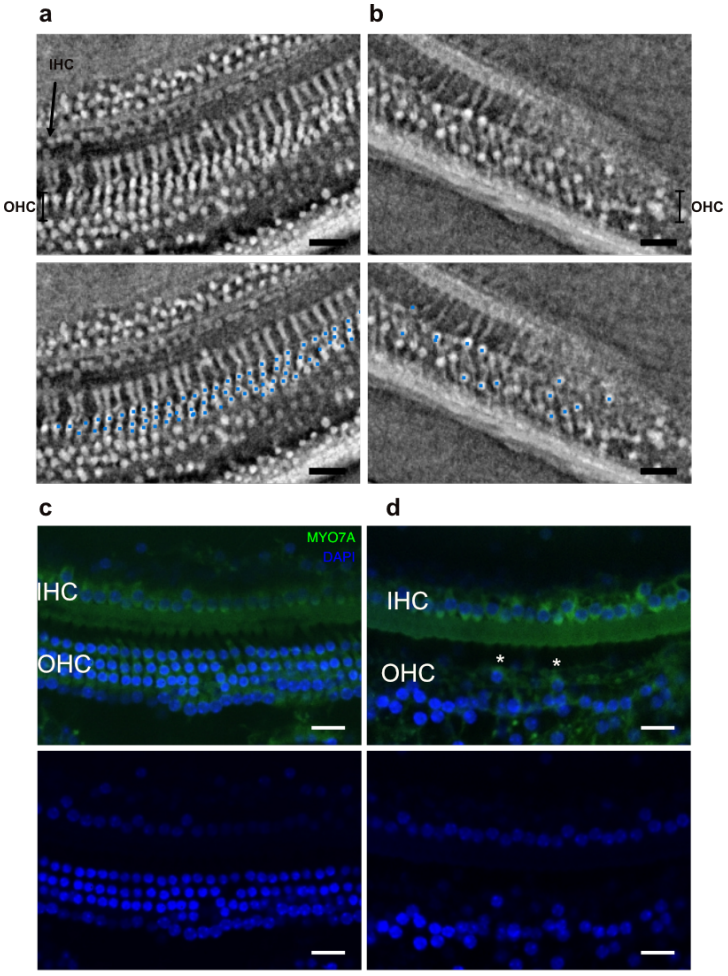

Figure 4. Images of the middle region of Sample 4, which was exposed to 100 dB SPL (a, c) and of Sample 5, which was exposed to 120 dB SPL (b, d) from SR-µCT (a, b) and immunofluorescence microscopy (c, d). The corrected labeled particles

are shown for SR-µCT on the average of three *z*-stack images. Immunofluorescence images show the fluorescence-labeled hair cells in green and the cell nuclei stained with DAPI in blue. MYO7A = myosin 7a. IHC = inner hair cells. OHC = outer hair cells. The scale bars are 20 µm. The arrow shows the area of the IHC in the SR-µCT images. The asterisks show the surviving hair cells.

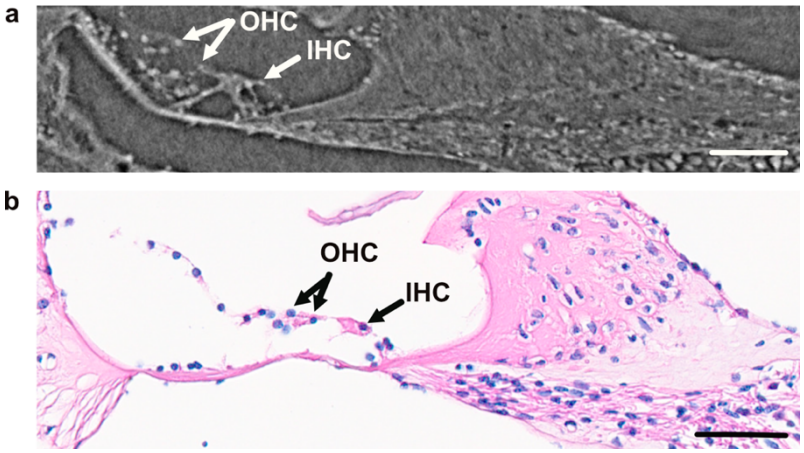

Figure 5. Cross-section of the middle cochlear region of Sample 6, which was exposed to 120 dB SPL. The sample was visualized with SR-µCT (a) or stained with hematoxylin-eosin stain and visualized with the slide scanner (b). IHC = inner hair cells. OHC = outer hair cells. The scale bars are 50 µm.

4. SUMMARY

The improved visualization of the cochlear cells in the inner ear was achieved with the SR-µCT technique applying our settings in comparison to previous reports, and also compared to the classical histology method. With the provided analysis settings, it was possible to distinguish healthy from damaged sensory epithelium. In the case of mild damage to the sensory epithelium, the hair cells were well recognized. In the case of mild damage to the sensory epithelium, the hair cells were well recognized. In the case of acute damage to the sensory epithelium with extensive loss of hair cells, the surviving cells were detected but distinguishing the type of cells remains challenging.

SR-µCT imaging is a promising method for the evaluation of the intact 3D cochlear structure, which allows for an improved diagnosis about the condition of damaged and undamaged sensory cells. The developed software substantially reduced the workload to identify hair cells in the middle basilar membrane region. Given the manual corrections now available, further software developments are possible that will support cell analysis for larger populations.

ACKNOWLEDGEMENTS

We thank the microscope core facility for their technical assistance. We would also like to acknowledge the members of the mouse facility for their assistance in animal care. The beamtime at the Anatomix beamline was granted by Synchrotron Soleil under proposal 20220597. Anatomix is an Equipment of Excellence (EQUIPEX) funded by the Investments for the Future program of the French National Research Agency (ANR), project NanoimagesX, grant no. ANR-11-EQPX-0031.

REFERENCES

[1] Varela-Nieto, I., Murillo-Cuesta, S., Calvino, M., Cediel, R., and Lassaletta, L., "Drug development for noise-induced hearing loss," Expert Opin Drug Discov, 15(12), 1457-1471 (2020).

[2] McPherson, D. R., "Sensory Hair Cells: An Introduction to Structure and Physiology," Integr Comp Biol, 58(2), 282-300 (2018).

[3] Montgomery, S. C., and Cox, B. C., “Whole Mount Dissection and Immunofluorescence of the Adult Mouse Cochlea,” J Vis Exp(107), (2016).

[4] Hutson, K. A., Pulver, S. H., Ariel, P., Naso, C., and Fitzpatrick, D. C., “Light sheet microscopy of the gerbil cochlea,” J Comp Neurol, 529(4), 757-785 (2021).

[5] Müller, B., Lareida, A., Beckmann, F., Diakov, G., Kral, F., Schwarm, F., Stoffner, R., Gunkel, A. R., Glueckert, R., Schrott-Fischer, A., Fischer, J., Andronache, A., and Freysinger, W., “Anatomy of the murine and human cochlea visualized at the cellular level by synchrotron-radiation-based micro-computed tomography,” Proc. SPIE, 6318(38), 631805 (2006).

[6] Rau, C., Hwang, M., Lee, W. K., and Richter, C. P., “Quantitative X-ray tomography of the mouse cochlea,” PLoS One, 7(4), e33568 (2012).

[7] Richter, C.-P., Liddy, W., Vo, A., Young, H., Stock, S., Xiao, X., and Whitlon, D., “Evaluation of neural cochlear structures after noise trauma using x-ray tomography,” Proc. SPIE, 9212, (2014).

[8] Richter, C.-P., Tan, X., Young, H., Stock, S., Robinson, A., Byskosh, O., Zheng, J., Soriano, C., Xiao, X., and Whitlon, D., “A comparison of classical histology to anatomy revealed by hard x-rays,” Proc. SPIE, 9967, (2016).

[9] Richter, C. P., Young, H., Richter, S. V., Smith-Bronstein, V., Stock, S. R., Xiao, X., Soriano, C., and Whitlon, D. S., “Fluvastatin protects cochleae from damage by high-level noise,” Sci Rep, 8(1), 3033 (2018).

[10] Lareida, A., Beckmann, F., Schrott-Fischer, A., Glueckert, R., Freysinger, W., and Muller, B., “High-resolution X-ray tomography of the human inner ear: synchrotron radiation-based study of nerve fibre bundles, membranes and ganglion cells,” J Microsc, 234(1), 95-102 (2009).

[11] Iyer, J. S., Zhu, N., Gasilov, S., Ladak, H. M., Agrawal, S. K., and Stankovic, K. M., “Visualizing the 3D cytoarchitecture of the human cochlea in an intact temporal bone using synchrotron radiation phase contrast imaging,” Biomed Opt Express, 9(8), 3757-3767 (2018).

[12] Li, H., Helpard, L., Ekeroot, J., Rohani, S. A., Zhu, N., Rask-Andersen, H., Ladak, H. M., and Agrawal, S., “Three-dimensional tonotopic mapping of the human cochlea based on synchrotron radiation phase-contrast imaging,” Sci Rep, 11(1), 4437 (2021).

[13] Weitkamp, T., Scheel, M., Perrin, J., Daniel, G., King, A., Le Roux, V., Giorgetta, J. L., Carcy, A., Langlois, F., Desjardins, K., Menneglier, C., Cerato, M., Engblom, C., Cauchon, G., Moreno, T., Rivard, C., Gohon, Y., and Polack, F., “Microtomography on the ANATOMIX beamline at Synchrotron SOLEIL,” Journal of Physics: Conference Series, 2380(1), 012122 (2022).

[14] Desjardins, D., Carcy, A., Giorgetta, J., Menneglier, C., Scheel, M., Weitkamp, T., "Design of Indirect X-Ray Detectors for Tomography on the Anatomix Beamline." 355–357.

[15] Maaten, L. v. d., Postma, E. O., and Herik, J. v. d., [Dimensionality Reduction: A Comparative Review] Tilburg University Technical Report, TiCC-TR, (2009).

[16] Kwan, C. C., Tan, X., Stock, S. R., Soriano, C., Xiao, X., and Richter, C. P., “Microanatomy of the cochlear hook,” Proc. SPIE, 10391, (2017).